3

Statistical Analysis in Homopolymeric Surfaces

Eralci M. Therézio[1], Maria L. Vega[2],
Roberto M. Faria[3] and Alexandre Marletta[1]
[1]*Universidade Federal de Uberlândia, Instituto de Física*
[2]*Universidade Federal do Piauí, Departamento de Física*
[3]*Universidade de São Paulo, Instituto de Física de São Carlos*
Brazil

1. Introduction

Surface topology investigation of luminescent polymeric films is a promising research area due to the interest in their technological application, mainly to large-area electroluminescent displays (Holzera et al., 1999). Surface topology of organic flexible materials is generally controlled by a chemical and physical process, the polymer coatings are generally heterogeneous, and the most significant changes occur in the nanometer scale (Gobato et al., 2002). The Atomic Force Microscopy (AFM) technique, in special, has made significant experimental contributions to three-dimensional imaging with high-resolution in a sub-nanometer scale, without specific sample preparation (Bar et al., 1998; Binnig et al., 1986; Gua et al., 2001). In soft biological or polymeric materials, the permanent contact of the tip produces irreversible deformation, modifying the surface topology (Magonov & Whangbo, 1996; Weisenhorn et al., 1992). To minimize these deformations, the AFM tapping mode was introduced as a non-destructive technique (Marti et al., 1999). In general, AFM systems include commercial software to control the probe and capture process, and analyze surface images such as height or phase. The subjective analysis of AFM images that sometimes depends on the high quality of the experimental data is commonly found in the literature. For example, quantitative analysis, uniformity, fractality, interface, nanostructure, composition, and others cannot be accomplished. The difficulty in performing the quantitative characterization of the surface increases during homopolymer films surfaces investigations, due to macro-molecule interpenetration, thus forming a very complex system (Marletta et al., 2010).

In this chapter, we focus on the study of surface homopolymer films, introducing first and second order statistics analysis. Poly(*p*-phenylene vinylene) films were investigated since they are easily processed by the casting technique. Casting PPV films were processed by a conventional precursor polymer route and thermal annealed at 230°C, under vacuum (10-3 mbar) (Marletta, 2000). AFM images were performed by the commercial *NanoScope® IIIa Multimode ™ of Digital instruments,* Santa Bárbara, CA, in a tapping mode. The first order statistical analysis was used to quantify the surface's topology, by calculating surface height distribution and roughness distribution moments mean squares, Skewness, and Kurtosis. Additional analysis was performed by a Scanning Probe Image Analysis (SPIA) (Costa et al., 2003) customized program to obtain the number of peaks, using the

maximum regional concept and distances between selected peaks. The second order statistical analysis was used to calculate the 1D height auto-covariance function of determined surface nanostructures. In addition, we have discussed the possibility to correlate the scattering of lights and the surface´s roughness. Finally, surface changes due to photo-bleach effects, oxidation phenomena, caused mainly by the oxidative processes, were investigated.

2. Statistical analysis of topologic surfaces

2.1 First-order statistical analysis

A random rough surface can be described by defining its height function, $h = h(\vec{r})$. The height h on a surface position $\vec{r} = (x, y)$ is obtained relatively to the mean height ($\overline{h}$), and the simplest approach to describe the surface is through height distribution $p(h)$. It gives the probability to find the height h between h and $h+dh$ at any point $(\vec{r})$ on the surface, and is positive and normalized as (Thomas, 1999; Zhao et al., 2001):

$$\int_{-\infty}^{+\infty} p(h)\,dh = 1 \tag{1}$$

It is important to emphasize that the purely random process, i.e. the random surface height distribution, is generally described by a Gaussian function. However, different statistical processes may be related to the treatment or growth mechanism of the surfaces. It is important to stress that the height distribution $h = h(\vec{r})$ was obtained by the SPIA program (Costa et al., 2003), where $\overline{h} = 0$. The first step to check whether the surface will be flat and/or rough, is through roughness measurement. The most used AFM technique is the roughness mean square (σ_{RMS}) (Palasantzas, 1993; Simpson et al., 1999), and the profile of the height distribution $p(h)$ is quantified by the value of the central moment, which is defined as (Zhao et al., 2001):

$$\sigma_n = \int_{-\infty}^{+\infty} \left(h - \overline{h}\right)^n p(h)\,dh\,. \tag{2}$$

The 1st-order moment is the height average: $\sigma_1 = \overline{h}$; the 2nd-order moment of the variable h is the root-mean-square (RMS) roughness (σ_{RMS}), which is given by:

$$\sigma_{RMS}^2 = \sigma_2 = \int_{-\infty}^{+\infty} \left(h - \overline{h}\right)^2 p(h)\,dh\,. \tag{3}$$

σ_{RMS} describes the fluctuations around the mean value $\overline{h}$, as the surface height approaches to random behavior, σ_{RMS} tends towards the width of the Gaussian distribution.

$$p(h) = \frac{1}{\sqrt{2\pi\Delta^2}} \exp\left(-\frac{(h-\overline{h})^2}{2\Delta^2}\right) \tag{4}$$

Figure 1 shows the typical height distribution for normal surfaces and a surface covered with bumps and pits. However, it is important to emphasize that different rough surfaces can have the same $p(h)$ and σ_{RMS}, but different height fluctuation frequency.

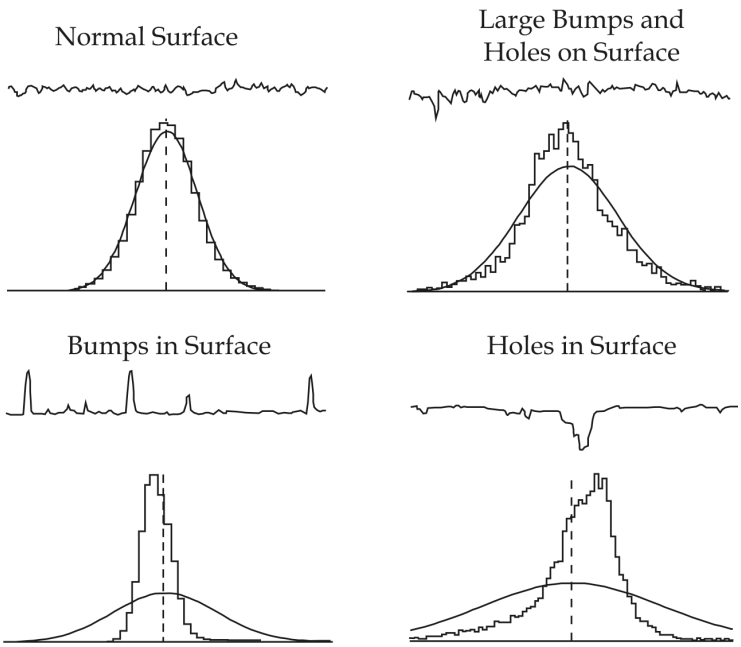

Fig. 1. Typical height distribution functions and equivalent Gaussians for a normal surface and a surface covered with bumps and pits (Bennett & Mattsson, 1999).

The higher-order moments give us more information about the surface height distribution, which is useful for analyzing surfaces in more detail. The Skewness (SK) is the 3rd-order moment given by:

$$\sigma_{SK} = \frac{\sigma_3}{\sigma_{RMS}^3} = \frac{1}{\sigma_{RMS}^3} \int_{-\infty}^{+\infty} \left(h - \bar{h}\right)^3 p(h)\,dh\,. \tag{5}$$

And σ_{SK} is sensitive to the asymmetry of the distribution. The Gaussian distribution has Skewness equal to zero, since it presents equally distributed peaks and valleys. Height distribution with negative Skewnees ($\sigma_{SK} < 0$) is due to a larger number of valleys and that with positive Skewnees ($\sigma_{SK} > 0$) is attributed to the larger number of peaks. By and large, this parameter gives an indication of the existence of a deep valley or sharp peaks. The 4th-order moment defines the Kurtosis (KU), given by

$$\sigma_{KU} = \frac{\sigma_4}{\sigma_{RMS}^4} = \frac{1}{\sigma_{RMS}^4} \int_{-\infty}^{+\infty} \left(h - \bar{h}\right)^4 p(h)dh\,. \tag{6}$$

σ_{KU} is the measurement of the height distribution sharpness, and it describes the randomness of the surface related to that perfectly random surface (Gaussian distribution), where $\sigma_{KU} = 3$. For $\sigma_{KU} > 3$, the distribution is platykurtic (mild peak) and for $\sigma_{KU} < 3$ the distribution is leptokurtic (sharp peak). The parameters σ_{RMS} (eq. 3), σ_{SK} (eq. 5), and σ_{KU} (eq. 6) are dependent on the on the measurements conditions such as: a) scanning size, b) lateral

and vertical resolution and, c) sampling density (Bennett & Mattsson, 1999; Thomas, 1999; Zhao et al, 2001).

2.2 Second-order statistical analysis

First-order statistics also gives information about the surface height at the individual position $\vec{r}$, that is, it does not reflect the correlation between the two different points $\vec{r}_1$ and $\vec{r}_2$. To take into account such specific situation in *homopolymers*, we introduced the second-order statistics, by calculating the height auto-covariance function $G(\vec{r}_1,\vec{r}_2)$, defined as (Zhao et al., 2001):

$$G(\vec{r}_1,\vec{r}_2)=\int_{-\infty}^{+\infty}\int_{-\infty}^{+\infty} h_1 h_2 p(h_1,h_2;\vec{r}_1,\vec{r}_2)\,dh_1 dh_2 \ . \tag{7}$$

Equation 7 gives the probability to find the height h_2 at $\vec{r}_2$ provided that we have the height h_1 at $\vec{r}_1$. For the homogeneous and isotropic rough surface, almost a normal surface, we consider that the $G(\vec{r}_1,\vec{r}_2)$ depends only on the distance between $\vec{r}_1$ and $\vec{r}_2$

$$G(\vec{r}_1,\vec{r}_2)=G(\rho)\,, \tag{8}$$

where $\rho=|\vec{r}_1-\vec{r}_2|$.

is the quantity and ρ is the translation coordinate, sometimes called the lag or the slip. For ρ = *0*, *G(ρ)* is equal to the variance of the surface height ($G(0)=\sigma_{RMS}^2$). For a random rough surface, the height auto-covariance function (*G(ρ)*) decreases to zero when the lateral distance increases ($\rho\to\infty$). In the first case, the shape of the function *G(ρ)* depends on the type of random surface and the distance over which two points become uncorrelated. The lateral correlation length ξ of an auto-correlation function defines the representative lateral dimension of the rough surface or the radius where two points cannot be considered correlated any more. The intensity of the correlation is defined as the radius where the function decays to $1/e$ of its zero-value:

$$G(\xi)=\frac{G(0)}{e}=\frac{\sigma_{RMS}^2}{e}\ . \tag{9}$$

Useful height auto-covariance functions are exponential (Eq. 10a), Gaussian (Eq. 10b), and self-affine (Eq. 10c) (Bennett & Mattsson, 1999; Palasantzas, 1993; Thomas, 1999). These functions are quite useful to describe surface topology. For example, $G(\rho)$ displays harmonic oscillation (sine or cosine) correlated with the surface periodic structure in a nanoscale dimension.

$$G(\rho)=G(0)\exp\left(-\frac{\rho}{\xi_{\exp}}\right), \tag{10a}$$

$$G(\rho)=G(0)\exp\left(-\frac{\rho^2}{\xi_G}\right), \tag{10b}$$

$$G(\rho) = G(0)\exp\left[-\left(\frac{\rho}{\xi_a}\right)^{2\alpha}\right]. \quad (10c)$$

In surface scattering theory, the position of the outgoing light is not necessarily the same as that of the incoming position. In this chapter, we consider that the light emitted by the PPV is scattered on the surface film/air and the light analyzed is obtained outside the material. It is possible to determine this interface's scattering intensity quantitatively from the correlation function of the rough surface profile. Using the inverse Fourier transform of the function $G(\vec{r}_1, \vec{r}_2)$ and the height auto-covariance function (Eq. 7), we obtain the following expression (Assender et al., 2002):

$$\langle I_s(\xi,\eta)\rangle = CTE * R * \iint_A G(\vec{r}_1, \vec{r}_2) \times \exp\left\{-\frac{2\pi i}{\lambda f}(\xi r_1 + \eta r_1)\right\} dr_1 dr_2 \quad (11)$$

where ξ and η are local variables, $R = \exp\left[-\left(\frac{4\pi\sigma_{RMS}}{\lambda}\right)^2\right]$ is the reflectance of the surface, σ_{RMS} is the root-mean-square roughness (eq. 3), λ is the scattered wavelength, $CTE = \frac{E_0^2 4k_Z^2}{2A^2 Z_W}$ is the constant, E_0 is the amplitude of the plane wave with air resistance $Z_W = \sqrt{\frac{\mu\mu_0}{\varepsilon\varepsilon_o}} \approx 377\Omega$, $\mu(\mu_0)$, k_z is the wavelength number, and A is the area of the laser excitation. Considering the homogeneous and isotropic rough surface (eq. 8), i.e., normal surface, we can rewrite the equation 10, by considering the maximum scattering intensity at $\xi = 0$ and $\eta = 0$ for the light outcome in the interface polymer/air and the normal surface approximation (eq. 8) as:

$$\langle I_{MAX}\rangle = \langle I(\xi = 0, \eta = 0)\rangle \propto \frac{R}{\sigma_{RMS}^2} \iint_A G(|\vec{r}_1 - \vec{r}_2|) dr_1 dr_2 \quad (12)$$

Where *G(ρ)* is the height auto-covariance function.

3. Casting PPV films

In this section, we will present the topological and optical study of casting PPV films in regards to thickness, stretching, and photo-blanching effects.

3.1 Topological analysis

By using 1st-order statistical analysis of surface homopolymer films, it is possible to investigate thickness effects on surface topology. It is important to emphasize that the phase image does not contribute, in the present study, with any additional information. Casting PPV films were processed from a conventional precursor polymer route, thermal annealed at 230°C, under vacuum (10^{-3} mbar), and thickness of 0.4, 0.9, 2.2, and 3.2 μm.

Figure 2 displays AFM height images, in a 10x10 nm² area for casting PPV films thickness of 0.4 μm (Fig. 2a) and 3.2 μm (Fig. 2b). A simple visual inspection shows a lot of peaks with height of about 50.0 nm for the thick film. However, the topology of a thin film is more homogeneous. So, what is the height distribution profile? Do the highest peaks represent a significant area on the film? What are the changes on the surface topology? Well, to answer these questions, we quantified the images using the 1st-order statistical analysis.

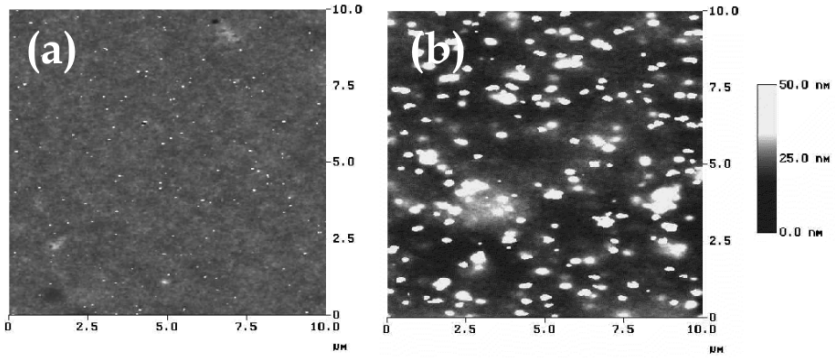

Fig. 2. AFM height image for *casting* PPV films with different thickness: (a) 0.4μm and (b) 3.2 μm.

Figure 3a and 3b shows the height histogram for 0.4 μm and 3.2 μm films, respectively, in which we can observe considerable dispersion of heights for the thickest film. One has thinner films, with less than 4.5% of peaks' heights (between 25 and 100 nm). As for thick films, the percentage increases considerable to 67.6%, in the same range. Latter data is not consistent with the visual observation of the AFM image! It is important to stress that the histogram in Figure 3 is a direct count of the heights of the AFM image in Figure 2. That type of histogram does not allow us to infer about the height distribution *p(h)* and to compare it with the types in Figure 1.

In order to improve the quantitative analysis of the height distribution, figure 4 plots the *p(h)* (Eq. 1) height distribution considering $\sigma_1 = \bar{h} = 0$ for thickness films of 0.4 μm (Fig. 2a) and 3.2 μm (Fig. 2b). It is interesting to observe the profile of both histograms where the thinnest film (Fig. 2a) is close to a normal surface and the thicker film is close to bumps on the surface (Fig. 1). The simple histogram analysis in Figure 2 is not able to demonstrate the behavior conclusion. To quantify the profile of *p(h)* (Figure 4), we calculated the values of σ_{RMS} (Eq. 3), σ_{SK} (Eq. 4), and σ_{KU} (Eq. 5). It is important to emphasize that these parameters depend on the AFM experiment, i.e., scanning size and lateral and vertical resolution (Bennett & Mattsson, 1999; Thomas, 1999; Zhao et al., 2001). Table 1 shows the evolution of the parameters for each sample. By increasing film thickness, the σ_{RMS} rises considerably, according to the AFM image in Figure 2b. The σ_{SK} parameter does not change significantly and presents relative low value (~3-5), closer to a normal surface for all samples. σ_{KU} decreases significantly when sample thickness increases, indicating the presence of sharp peaks on the surface. Finally, we can consider the values for σ_{SK}, σ_{KU}, and σ_{RMS} in Table 1 as closer to the Gaussian distribution ($\sigma_{RMS} = \Delta$, $\sigma_{SK} = 0$, and $\sigma_{KU} = 3$), for all samples.

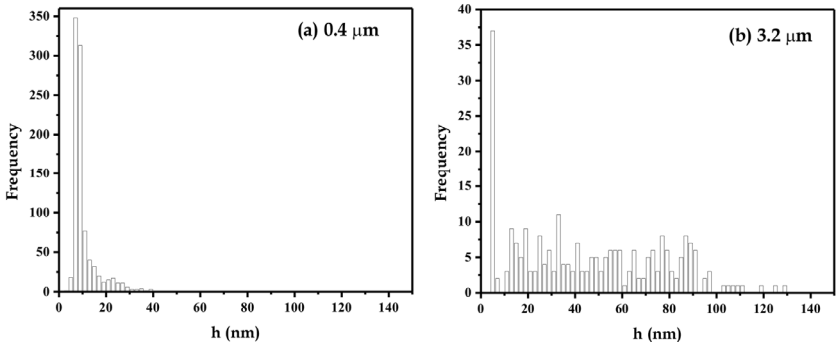

Fig. 3. Height histogram of AFM images in Figure 2, with thickness of (a) 0.4μm and (b) 3.2 μm.

Thickness (μm)	0.4	0.9	2.2	3.2
σ_{RMS} (nm)	1.5 ± 0.1	7 ± 4	10 ± 1	14 ± 2
σ_{SK}	5 ± 1	3.6 ± 0.3	3.1 ± 0.1	3 ± 1
σ_{KU}	54 ± 5	22 ± 3	13 ± 3	13 ± 4

Table 1. First-statistical parameters: roughness (σ_{RMS}), Skewness (σ_{SK}) and Kurtosis (σ_{KU}) in function of film thickness of 0.4, 0.9, 2.2, and 3.2 μm.

Fig. 4 (continuous line) shows data adjustment for *p(h)*, using the equation. The mean square root between the histogram and the fit, using the Gauss function, is about 97% for all samples, according to the approach mentioned above. Figures 4a and 4b show the contribution of high height values (|h|>25nm) for films with thickness of 0.4 and 3, 0% and 9% respectively. These findings corroborate with the discussion above mainly for thicker films, where the number of peaks above 25 nm is smaller than the calculation using the height histogram in Fig. 3. Finally, we can conclude that surfaces are essentially topological structured at low height values (< 25nm) and the thickness of PPV casting films, after being processed, does not change the polymeric surface significantly.

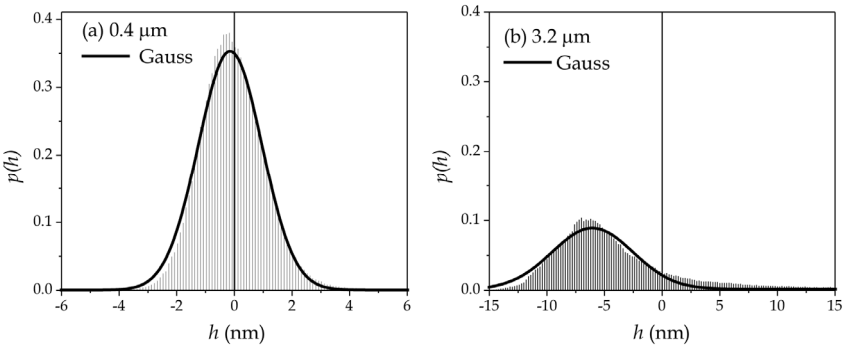

Fig. 4. Height distribution *p(h)* for film thickness 0.4 μm (a) and 3.2 μm (b). The continuous line represents the adjustments using Gaussian function (Eq. 4).

We have also analyzed the distance between the first adjacent selected peaks, 50, 100, 150, 200, and 250, using the methodology developed by Costa et. Al., 2003. In summary, the count is performed by slicing the AFM image along its thickness in a step $\Delta Z=(h_{max}-h_{min})/n$, where n is the number of slices, adding new peaks after each slice. The mean distance between first-neighbor introduces a number of combinations equal to $n!/(2!\ (n-2)!)$. It shows, mainly, how uniform the peak distribution is on the film surface. The mean distance <d> was calculated as:

$$\langle d \rangle = \frac{\sum_j d_j \cdot f_j}{\sum_j f_j} \tag{13}$$

where d_i is the distance between two selected peaks with frequency f_i. Figure 5 shows the mean distance for the nearest selected peaks for all samples, considering ΔZ = 0.1nm. The value of <d> (Eq. 13) and the mean height $\sigma_1 = \bar{h}$ (Eq. 2) are also listed in Table 2.

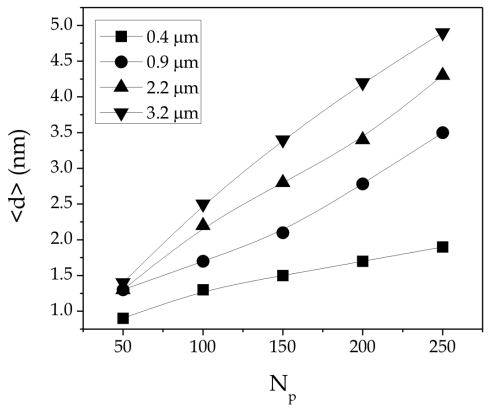

Fig. 5. Average distance <d> (Eq. 9) in function of the first-neighbor selected peaks, 50, 100, 1500, 200, and 250, for sample thickness of 0.4, 0.9, 2.2, and 3.2 μm.

Thickness (μm)	$\bar{h}$ **(nm)**	$\langle d \rangle$ **(nm) -** ***First neighbor***				
		50	*100*	*150*	*200*	*250*
0.4	12.6	0.9	1.3	1.5	1.7	1.9
0.9	13.7	1.2	1.7	2.1	2.5	2.9
2.2	21.2	1.3	2.2	2.8	3.4	4.1
3.2	28.5	1.4	2.5	3.4	4.2	4.9

Table 2. Mean height $\sigma_1 = \bar{h}$ (Eq. 2) and average distance <d> (Eq. 15) of adjacent selected peaks in function of the number of the first neighbor: 50, 100, 150, 200, and 250 for all casting PPV films.

The distance between adjacent peaks was obtained by choosing 5 positions on AFM images, randomly. A monotonic increase of the mean distance between first-neighbors (selected

peaks) where the number of peaks rises from 50 to 250 can be observed. This last result is consistent with the above observation, where casting PPV films do not change the surface topology significantly due to thickness. This last result is confirmed by observing the peaks with height equal to 50 nm (white pixels) in the AFM image in Fig 2. The mean height parameter is equal to 12.6 and 28.6 nm, where the thickness is equal to 0.4 and 3.2 μm, respectively. In fact, the parameter allows us to confirm the presence of a larger number of high height peaks in thick PPV films (see Fig 4). We can infer that the surface is more heterogeneous when the thickness increases.

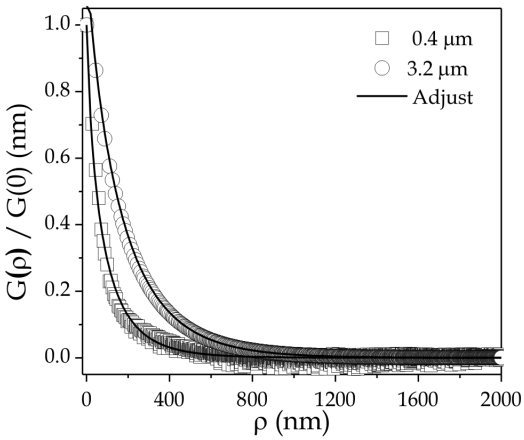

Fig. 6. Height auto-covariance curves for the AFM image (Fig. 1) for casting PPV films thickness of 0.4 μm (open cube) and 3.2 μm (open circle). The continuous line represents the adjustment using a self-affine equitation (Eq. 10c).

To confirm the previous finding that the statistical analysis of first and second order, where the thickness does not change significantly the surface topology of casting PPV films, we estimated the maximum of the film light scattering $<I_{MAX}>$ (Eq. 10). The result of the calculation for all samples is presented in Table 3. A non-significant variation of the scatter intensity was obtained, which corroborated with the experimental measurement of photoluminescence (PL), excitation 457 nm of the argon ion laser, and normalized at the thickness (NPL) (see Fig 7). Both NPL spectra present the same line shape and approximately the same intensity, confirming the data presented in Table 3.

Thickness (μm)	0.4	0.9	2.2	3.2
$G(0)$	2.3 ± 0.1	59 ± 4	142 ± 6	203 ± 10
$G(0)/e$	0.9 ± 0.1	22 ± 2	42 ± 3	75 ± 5
ξ_a (nm)	72 ± 5	152 ± 7	158 ± 7	163 ± 8
α	0.37 ± 0.02	0.41 ± 0.03	0.43 ± 0.03	0.45 ± 0.03
$\langle I_{MAX} \rangle$	0.028	0.027	0.026	0.025

Table 3. Best adjustment parameters for casting PPV films thickness of 0.4, 0.9, 2.2, and 3.2 μm, using the self-affine function and the maximum scattering intensity $<I_{MAX}>$ (Eq. 12).

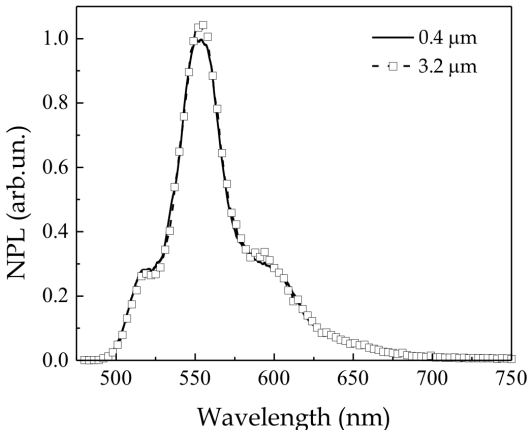

Fig. 7. Normalized photoluminescence spectra (NPL) for casting PPV films with thickness of 0.4 μm (line) and 3.2 μm (square-line). Spectra were normalized by the thickness.

3.2 Stretched casting PPV film

Polymer light emission diodes are generally processed as a thin film by the spin-coating technique on a transparent metal. As intrinsic characteristics of the spin-coating technique, the films are isotropic and the emission does not show linear polarization, as well. This is particularly interesting for the information industry (Cimrová et al., 1996). Polymers films are mechanically stretched easily, and the macromolecules are aligned, inducing anisotropy along the stretching direction, and the optical properties, in particular luminescence, are strongly affected by molecular anisotropy (Alliprandini et al., 2009; Therézio et al., 2011a, 2011b). This finding is corroborates with the fact that the emission polarization has a direct relationship with the orientation of the molecular transition dipole (electric) moment. Moreover, in most of the works done on emission polymers properties, the photo-physical process of energy transfer between conjugated polymers are poorly understudied due to the complex morphology of these materials. In the present section, we investigate stretch effects on surface topology of casting PPV films deposited on poly(vinylidene fluoride) (PVDF) tapes.

Fig. 8 displays AFM height images in a 10x10 nm^2 area for casting PVDF/PPV films stretched at 0% (ST0% - Fig. 8a), 50% (ST50% - Fig. 8b), and 100% (ST100% - Fig. 8c) in their length (axis y). Examples of height profiles for each AFM image are presented in Fig 8.A non-intentional alignment of the PPV casting film on a PVDF tape is observed (see Fig. 8a); the PVDF tape in their fabrication is stretched, and the surface ripple is expected, self-organizing the PPV chains due to the polymer/polymer interface. Where stretching was applied to ST50% and ST100% films, the alignment is more evident. The height profile in Fig. 8b and 8c shows a periodic oscillation perpendicular to the stretch direction. Next, the root-mean-square roughness (σ_{RMS}) increases as the perceptual of stretching increases; it is equal to 15, 21, and 30 nm for a stretching percentage equal to 0%, 50%, and 100%, respectively.

Figure 9 presents the height distribution (Eq. 1) for all AFM images in Fig. 8. For ST100% sample, the function $p(h)$ reduces considerably the width at half height, and it is closer to a Gaussian distribution (Eq. 4), $\chi^2 \sim 10^{-7}$. Table 4 lists the parameters obtained using equation 4.

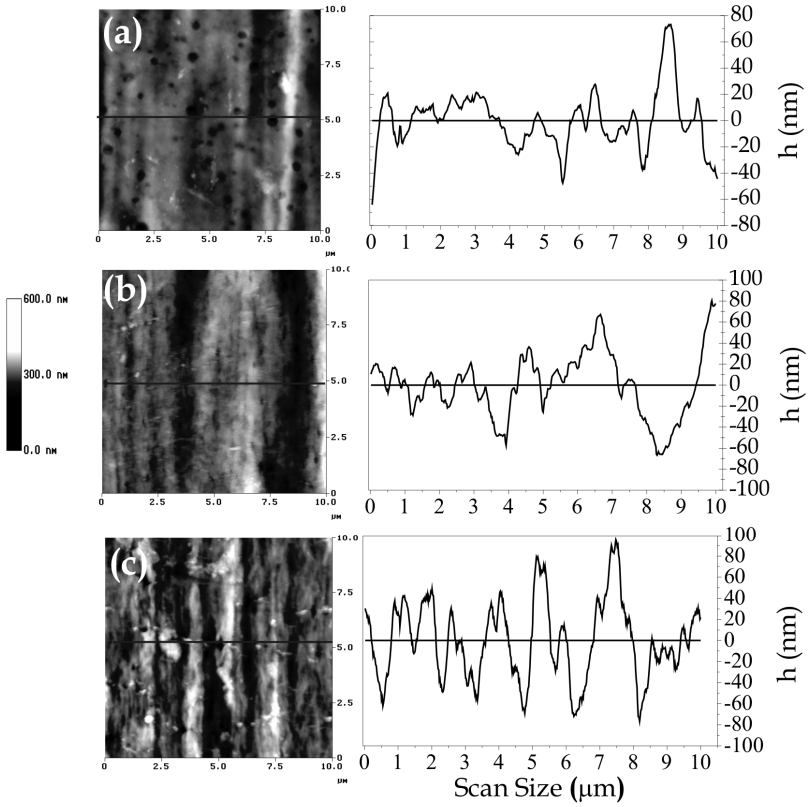

Fig. 8. AFM images (left) and height profile (right) for casting PVDF/PPV films stretched (a) 0%, (b) 50%, and (c) 100%.

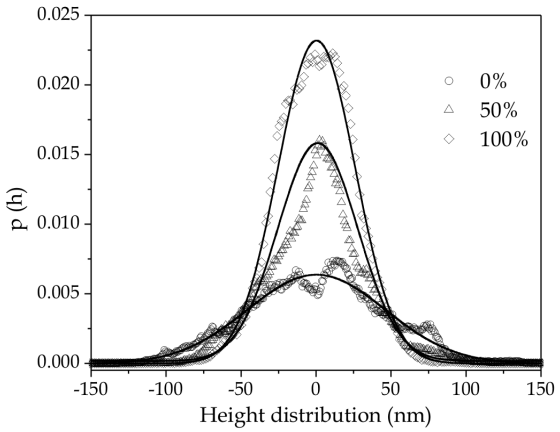

Fig. 9. Height distribution *p(h)* for ST0%, ST50% and ST100% films. The continuous line represents adjustments, using the Gaussian function (Eq. 4).

Sample	Stretching (%)	$\bar{h}$ (nm)	Δ(nm)
ST0%	0	0.22±0.04	92.1±0.9
ST50%	50	1.15±0.03	60.4±0.6
ST100%	100	1.74±0.01	51.5±0.2

Table 4. Best fit parameters of the height distribution p(h) for ST0%, ST50% and ST100% films in Figure 9.

By increasing the stretching perceptual, the first moment, $\sigma_1 = \bar{h}$, displays values near the normal surface, where $\sigma_1 \rightarrow 0$. This is corroborated with the half height (Δ) decrease shown in Table 4, for function *p(h)*.

The second statistical order was applied to the AFM images in Fig. 8, considering the approach of expression 7. Results are presented in Fig. 10. The white pixels in Fig. 10 represent heights with higher correlation. It is interesting to observe the presence of anisotropy in the direction of the stretching direction.

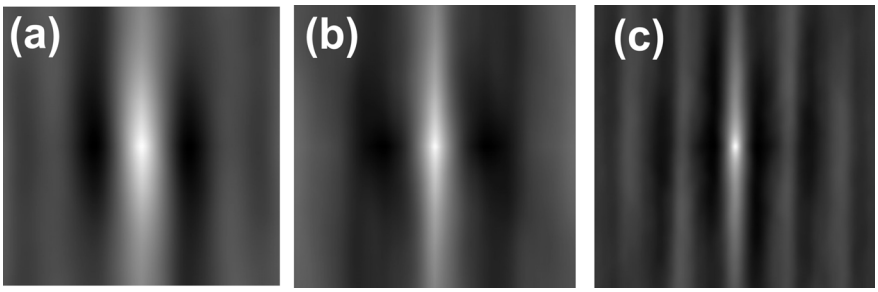

Fig. 10. Height auto-covariance image of casting PVDF/PPV films stretched at (a) 0%, (b) 50%, and (c) 100% for the AFM images in Fig. 8.

We can define the height-difference correlation function $g(\rho)$ as(Bennett & Mattsson, 1999; Marletta et al., 2010), by using the height auto-covariance function $G(\rho)$ (Eq. 7),:

$$g(\rho) = 1 - \frac{G(\rho)}{\sigma_{RMS}^2}. \tag{14}$$

Figure 11 displays the component of height-difference correlation for all samples. Fig.11a shows the component in perpendicular direction g(x) and Fig. 11b in parallel direction g(y) of the stretch direction (axis y). The main result is the periodic oscillation of the function g(x) for ST50% and ST100% films. Moreover, when the stretching increases (100%), the period of the oscillation decreases, in agreement with the images in Figure 10. This analysis allows for the verification of the anisotropy effects introduced due to mechanical stretching of PVDF/PPV film. For the component g(y), the correlation of the heights follows the behavior observed for casting PPV films, section 3.1, and a large length of non-correlated heights is observed. To quantify the correlation length, Table 5 presents the lateral correlation length parameters ξ (Marletta, 2010). The correlation length for non-stretched sample (ST0%) is different in both analyzed directions. In principle, casting films should not present that

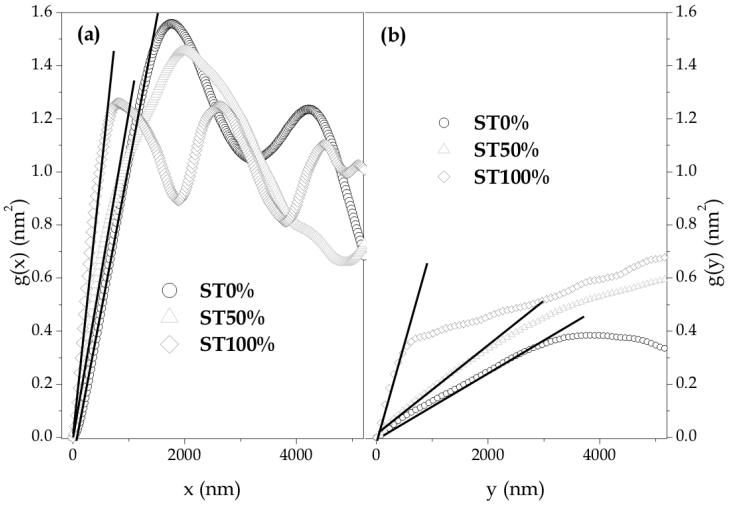

Fig. 11. (a) Perpendicular – *g(x)* and (b) parallel – *g(y)* components of height-difference correlation function for AFM image (Fig. 8) of casting PVDF/PPV films stretched at 0%, 50%, and 100%. Stretch direction is the axis y.

Sample	Stretching (%)	Direction	ξ_a (nm)	α
ST0%	0	x	623±5	0.97±0.02
ST50%	50	x	452±6	0.81±0.03
ST100%	100	x	260±2	0.99±0.3
ST0%	0	y	418±5	0.49±0.01
ST50%	50	y	273±3	0.47±0.02
ST100%	100	y	270±3	0.34±0.01

Table 5. Lateral correlation (for casting PVDF/PPV films of ST0%, ST50%, and ST100%.

difference. However, the AFM image (Fig. 8a) shows an initial anisotropy in a PPV film on a PVDF tape. By increasing the stretching percentage, that parameter decreases considerably, showing the strong dependence between both analyzed directions.

Finally, to confirm the anisotropy of the PPV moieties along the stretching direction, Fig. 12 presents the polarized absorbance (Fig. 12a) and the polarized emission (Fig. 12b). The enhancement in the absorbance and emission in the parallel direction, proving the presence of anisotropy, is evident.

3.3 Diffraction grating

In this section, we report and analyze the physical effects of the photo-oxidation reaction on PPV cast films, using the AFM technique. The experimental setup for the grating recording is shown in Fig. 13. A linearly polarized Ar ion laser beam, operating at 488 nm, is used to induce grating. This laser beam passes through a half-wave plate, to control its polarization,

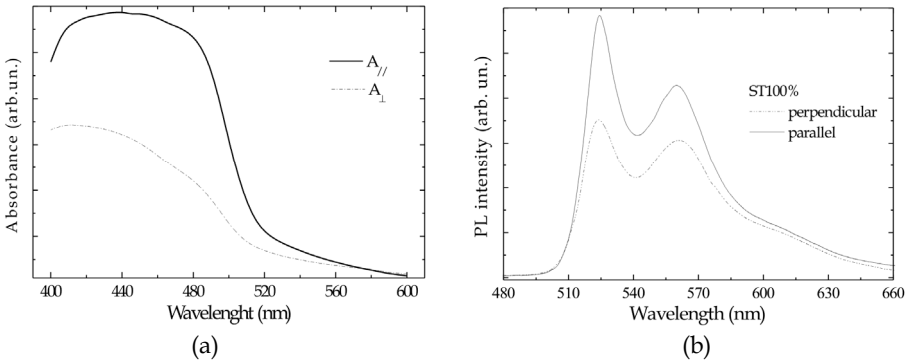

Fig. 12. (a) Polarized absorbance spectra for casting PVDF/PPV film stretchered at 100% (ST100%) parallel ($A_{//}$ - black line) and perpendicular ($A_{\perp}$ - red line) to the stretching direction. (b) Polarized photoluminescence spectra for casting PVDF/PPV film stretched at 100% (ST100%) parallel (black line) and perpendicular (red line) to the stretching direction.

and is expanded and collimated before shining the sample. Half of the collimated beam impinges directly the sample, while the other portion is reflected onto the sample from a aluminum coated mirror. The grating was recorded with s and p polarization. The intensity of the recording beam after the collimation system was 200 mW/cm², and the recording time was about 2 hours. The incident angle of the recording beams was selected at 10°, resulting in a grating spacing of about 2 μm.

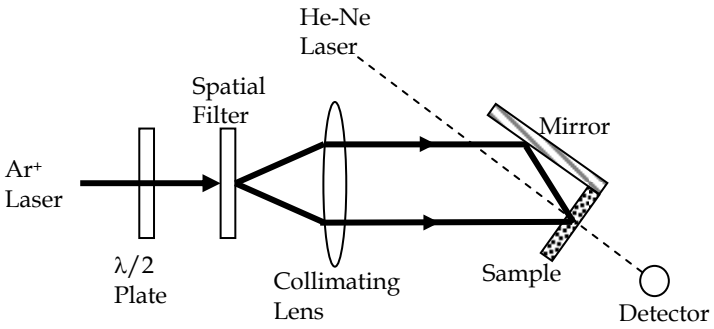

Fig. 13. Experimental setup of the holography diffraction grade recording.

Macroscopic modifications in the PPV surface were verified by using optic microscopy images. Fig. 14 shows the non-irradiated (NI) and irradiated (I) regions, clearly distinguishable in the AFM image, which was obtained by using a CCD camera coupled to the microscope, using the illumination in the transition setup. The majority of the light was transmitted in the irradiate region (I), in agreement with the absorption spectra (Gobato et al., 2002). In this macroscopic scale, the image shows qualitatively low non-homogeneity in both surface regions, with morphological defects (peaks) distributed randomly on the surface. Such morphological defects in the NI region were produced during the thermal conversion process.

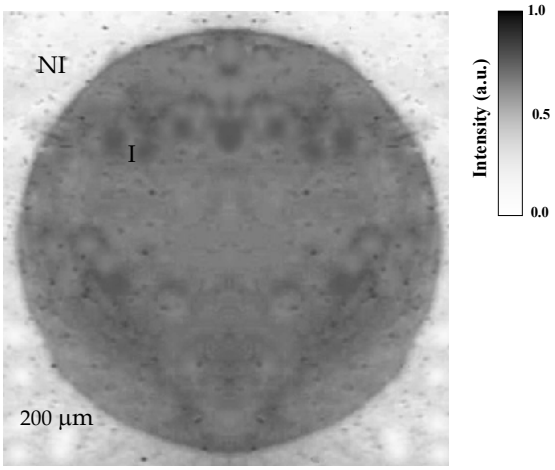

Fig. 14. Optic image of non-irradiate (NI) and irradiate (I) region.

Fig. 15 shows the PL spectra of the PPV film before (0 min) and after (35 min) the photo-irradiated exposure, using an Ar+ laser (458 nm) at 200 mW/cm^2 in atmospheric conditions. The PL-intensity increases 250% after being exposed to light, without significant changes in the spectral line shape. The inset in Fig. 15 shows the normalized PL-intensity enhancement, which reaches saturation for an exposition time of 30 min. This figure shows that the zero-phonon peak at about 516 nm (2.4 eV) and the vibronic progression in the low energy spectral range are unchanged in both spectra. During the irradiation, the ratio between the intensities of zero-phonon and the first-phonon replica peak (553 nm) is approximately constant and equal to 0.29. This value indicates a high electron-phonon coupling (Huang Rhys parameter), characteristic of the structural disorder, impaired by the molecular random packing of the cast deposition technique.

The presence of chemical structure degradation is evident in the absorption of the UV-Vis range and infrared (IR) measurements reported by Gobato et al., 2002. After light exposure, the absorption spectrum is blue shifted and the IR spectrum presents a major increase in 1690 cm^{-1} peak, identified as the carbonyl group (C=O) incorporation (Barford & Bursill, 1997; Chandross et al., 1994; Friend, et al., 1997; Onoda et al., 1990). This defects incorporation indicates chemical changes in PPV main chains, raising the PPV HOMO-LUMO band gap, with a reduction in the effective conjugation degree of the PPV.

Fig. 16 shows AFM images obtained by using the tapping mode for the non-irradiated (Fig. 16a) and irradiated (Fig. 16b) regions, indicated as NI and I in the Fig. 14, respectively. The simple visual analysis of these images shows a significant difference between both regions. The non-irradiated region shows a minor number of peaks with height greater than 25 nm, distributed randomly on the surface. The irradiated region presents a considerable increase in the number of peaks, with height greater than 25 nm, distributed more homogeneously on the surface. In the 10 μm AFM image scale, the non-irradiated region presents peaks with a diameter larger than irradiated region, as observed in the macroscopic image in Fig. 14.

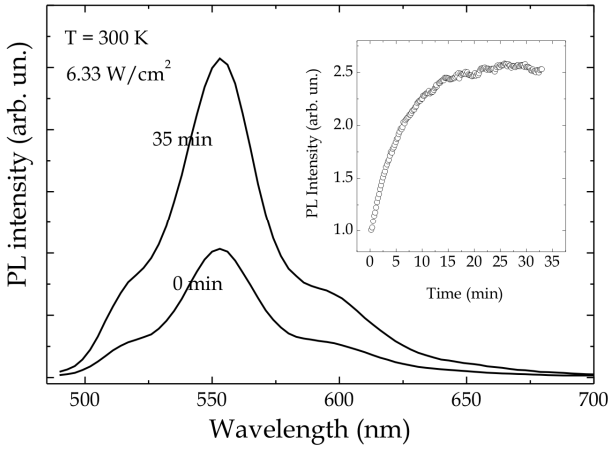

Fig. 15. PL spectra before (0 min) and after (35 min) photo-irradiation at 200 mW/cm² for a PPV cast film under environmental conditions. The insert shows the time evolution of the PL-intensity.

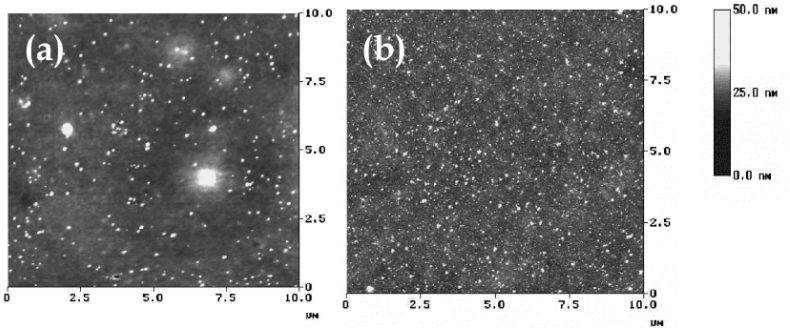

Fig. 16. AFM image in tapping mode of non-irradiate (a) and irradiate (b) regions.

The roughness is 4.0 nm in the non-irradiated and 2.8 nm in the irradiated region. These findings include surface changes induced during the laser exposure of the PPV film, but it is not enough to conclude that the irradiated surface is more homogeneous than the non-irradiated region. The surface analysis of polymeric films using a subjective AFM image analysis and the roughness parameter is difficult, once the phase image does not show additional information like in films composed by polymeric blends.

The new methodology proposed in this work is based on the quantitative analysis of AFM images using a statistical study of the peak height distribution and distance between peaks. A substantial increase in the total number of peaks, with the irradiated region presenting approximately 5 times more peaks (1.6×10^4) than the non-irradiate (3.3×10^3) is observed. Fig. 17 shows the distribution of peaks height in the irradiated (Fig. 17a) and non-irradiated (Fig. 18b) region. In both regions, the major contribution to the histogram is in the range between 6 and 14 nm. For these initial data, we can observe in the irradiated region that the peaks height fraction, superior to 12 nm and 18 nm in the non-irradiated region, are less than 1% of the total

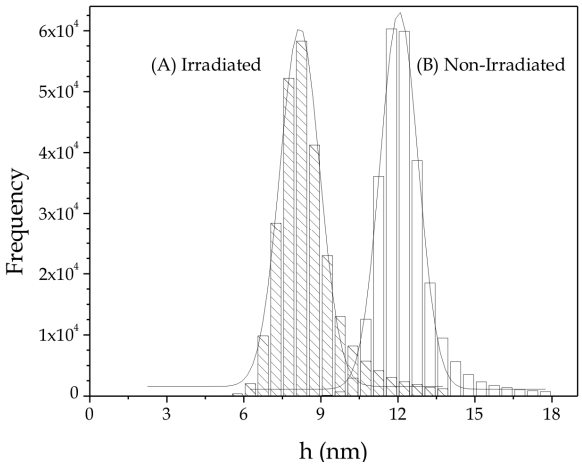

Fig. 17. Histogram of peak heights in irradiated (a) and non-irradiated (b) regions. Gaussian function was used to fit the distribution.

peaks on both surface. The histograms in Fig. 17 were adjusted using a Gaussian curve. The distribution width is narrow, with 1.5 nm in both regions, centralized at 12.1 nm and 8.2 nm, and the maximum is 1.2×10^5 and 1.0×10^5 for non-irradiated and irradiated regions, respectively. These findings show that the surfaces are not changed dramatically, with a small tendency to increase the surface disorder with the decrease of the peak height. In comparison with the AFM image in Fig. 16, we observe that the major contribution to the surface is centralized in the region with low peak heights (<15 nm), which is not perceived visually.

The distribution of the distance between peaks is plotted in Figure 18. Histograms were adjusted using a Gaussian curve and presented similar parameters. Distances between peaks, in both regions, are centralized at 5.1 μm and the width at 6.3 μm. The main difference is the amplitude of the distribution, which is one order greater for the irradiated region. These findings corroborate with the data obtained in Fig. 18, and the principal contribution to the surface morphology is in a nanometer scale that it is not perceived by the visual analysis of the AFM image in Figure 16.

When the PPV casting films were photo-irradiated for a short time, we observed an increase in the intensity of photoluminescence is observed. On the other hand, a long exposure to irradiation decreased the intensity. Both effects can be connected to the degradation process in the structure of the polymeric chain. By using a photo-oxidation process, we produced a diffraction grating in the PPV film. Fig. 19a shows the AFM diffraction grating image where alternating irradiated and non-irradiated regions can be observed. Similar surface relief grating formation has been observed in azopolymeric films, in which a driving force that depends on the gradient of the electric field and the local plasticization assisted by the trans-cis-trans photoisomerization is the mechanisms responsible for the molecular movimentation (Bian et al., 1999; Kumar et al., 1998). However, in the present work, the surface relief grating observed is due to a polymeric chain photo-oxidation, which causes changes in the PPV photo-luminescence, as mentioned before. This result can be used in light emitting display to store the information on the surface.

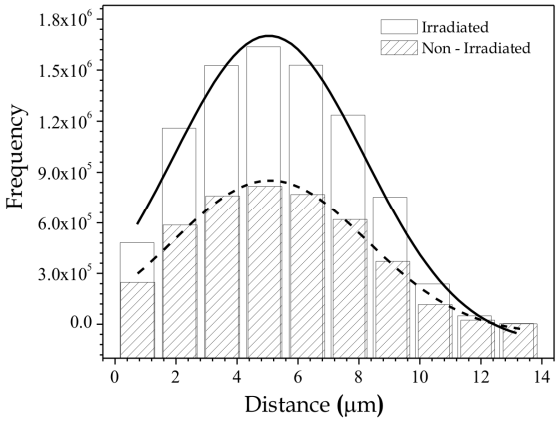

Fig. 18. Histogram of the distance between peaks in non-irradiated and irradiated regions. A Gaussian function was used to fit the distribution.

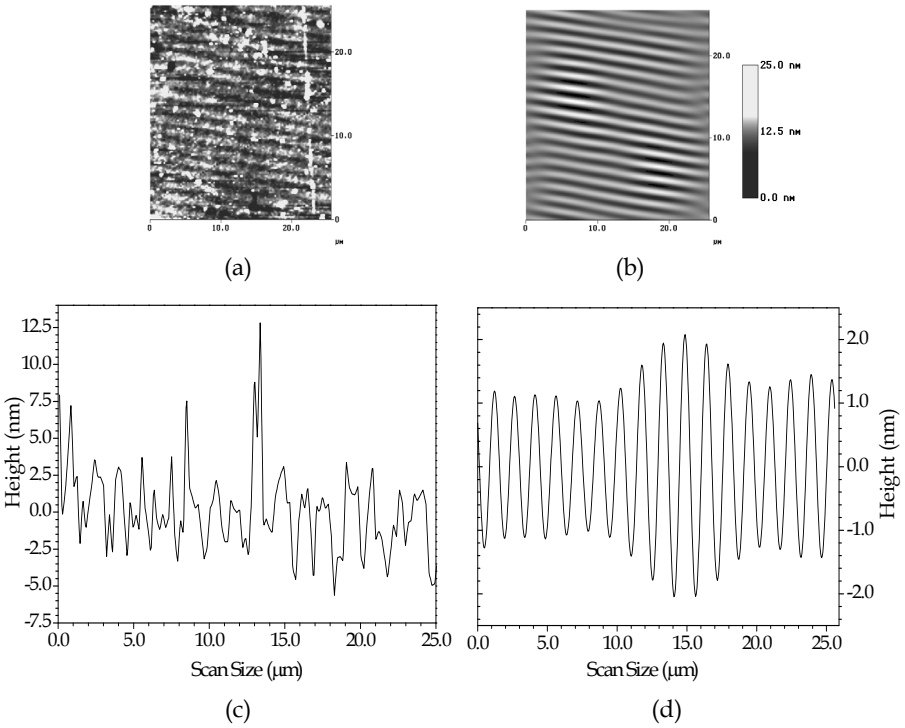

Fig. 19. (a) shows the AFM diffraction grating image alternating between irradiated and non-irradiated regions and (b) the AFM diffraction image obtained after the Fourier transform application explained in the experimental section. Figure (c) and (d) show the transversal section of the original AFM image (a) and the image obtained after the Fourier filtering (b), respectively.

Fig. 19a was obtained by carrying out the Fourier transforming explained in the experimental section. After the Fourier transforming shown in Fig. 19a, two bright points in the second and fourth quadrant were obtained. These points correspond to a frequency period of 1.6 μm. These values are related to the well-defined grating periodicity observed in the real image. These frequencies correspond to a regular standard of undulation in the real image. The grating periodicity found through the imaging processing method (1.6 μm) is similar to the one calculated in the experimental section (1.5 μm), revealing the reliability of the adopted image analyses. Figures 19c and 19d show the transversal section of the original AFM image and the image obtained after the Fourier filtering. The peak-peak height obtained is ~ 1.3nm for the original image and is 1.55nm for the Fourier filtered image.

The peak-valley height of the grating inscribed in this film through the photo-oxidation process as determined by AFM, is approximately 7.9 nm. This value is smaller than those usually obtained for surface relief grating in azo-doped films, which in general present amplitude of modulation of around 100 nm. Furthermore, surface relief grating formation is, in general, polarization dependent, being more efficient for p-polarized than for s–polarized light. No indication of such polarization dependence was observed in our experiments. This result leads to the conclusion that the grating formation process here presented here is probably a bulk process, in agreement with previous evidences.

In summary, the quantitative analyses show that the surface morphology is not affected significantly during the laser exposure process at low power. We observe that the visual analysis of the FM image is not sufficient since important features of the microscopic morphology for homogeneous polymeric PPV films cannot be distinguished visually. The use of an image statistical analysis and specific software showed the importance of quantifying the morphological parameters, the heights of pixels and the distances between peaks. By using this methodology, the image interpretation can replace the usual subjective visual analysis. The decrease in the σ_{RMS} parameter verified by using specially developed software indicates that the surface is not affected significantly and can be used to deposit metallic electrodes in the fabrication of polymeric light-emitting devices.

4. Conclusion

Surface statistical analysis of homoplymer films using height AFM images proved to be important to quantify the topological structure and to identify surface type. Thickness, mechanical modification, and photo-blanch effects on the surface topology of casting PPV film were explored in the present chapter, using first and second order statistical analysis. The simple observation of AFM images or height histograms is not able to infer the changes on the surface topology due to physical or chemical modifications. Through casting PPV films, we explore all potentiality of the mathematical tools introduced in section 2. In summary, the height distribution *p(h)* moments describe the type of the surface, normal surfaces and surface covered with bumps and pits, or a combination of them. The second statistical order describes the typical distance until the heights and the effects on, for example, scatter lights are correlated. Additional analysis, using the distance between adjacent peaks, can inform about surface homogeneity. It is important to emphasize that the development of new procedures or techniques to analyze AFM images is essential to improve the knowledge on surface topology and mechanical, electrical, and optical

properties of luminescent polymers. The study is not limited to a matter of scientific investigation. It became a matter of technological interest with applications in organic electronics.

5. Acknowledgment

This work had the financial support of FAPEMIG, CNPq, CAPES and INEO/MCT (Brazil). The authors are grateful to Professor Cléber Mendonça from *Instituto de Física de São Carlos* (USP, Brazil) for the use of the Institute's experimental facilities and to Carlos Alberto Rodrigues from *Departamento de Ciências Exatas* (UEFS, Brazil) for the use of the SPIA computing program facilities. The authors are grateful to Hugo Santos Silva a student from the *Grupo de Espectroscopia de Materias* (UFU, Brazil), for the text layout.

6. References

Alliprandini, P.; da Silva, G. B.; Barbosa Neto, N. M.; Silva, R. A. & Marletta, A. (2009). Induced Secondary Structure in Nanostructured Films of Poly(p-phenylene vinylene). *Journal of Nanoscience and Nanotechnology*, Vol.9, No.10, (Octuber, 2009) pp. 5981-5989, ISSN 1533-4880

Assender, H.; Bliznyuk, K. & Porfyrakis, V. How Surface Topography Relates to Materials' Properties. *Science*, Vol.297, No.5583, (August, 2002), pp. 973-976, ISSN 0036-8075

Bar, G. & Thomann, Y. (1998). Characterization of the Morphologies and Nanostructures of Blends of Poly(styrene)-block-poly(ethene-co-but-1-ene)-block-poly(styrene) with Isotactic and Atactic Polypropylenes by Tapping-Mode Atomic Force Microscopy. *Langmuir*, Vol.14, No.5, (February, 1998), pp. 1219–1226, ISSN 0743-7463

Barford, W. & Bursill, R. J. (1997) Theory of molecular excitons in the phenyl-based organic semiconductors . *Chemical Physics Letters*, Vol.268 , No.5-6 (April,1997), pp. 535-540, ISSN 0009-2614

Bennett, J. M. & Mattsson, L. (1999). *Introduction to surface Roughness and Scattering,* Optical Society of America, ISBN 1-55752-609-5, Washington DC, USA

Bian, S.; Williams, J. M.; Kim, D. Y.; Li, L.; Balasubramanian, S.; Kumar, J. & Tripathy, S. (1999). Photoinduced surface deformations on azobenzene polymer films. *Journal of Applied Physics*, Vol.86, No.8,(July, 1999), pp. 4498-4508, ISSN 0021-8979

Binnig, G.; Quate, C. F. & Gerber, Ch. (1986). Atomic Force Microscope. *Physical Review Letters*, Vol.56, No.9, (March, 1986), pp. 930–933, ISSN 0031-9007

Chandross, M.; Mazumdar, S.; Jeglinski, S.; Wei, X.; Vardeny, Z. V.; Kwock, E. W. & Miller, T. M. (1994). Excitons in poly(para-phenylenevinylene). *Physical Review B: condensed matter and materials physics*, Vol. 50, No. 19, (November, 1994), pp. 14702–14705, ISSN 1098-0121

Costa, L. D. F.; Rodrigues, C. A.; Souza, N. C. D. & Oliveira, O. N. Statistical Characterization of Morphological Features of Layer-by-Layer Polymer Films by Image Analysis. *Journal of Nanoscience and Nanotechnology*, Vol.3, No.3, (June, 2003), pp. 257-261, ISSN 1533-4880

Cimrová, V.; Remmers, M.; Neher, D. & Wegner, G. (1996). Polarized light emission from LEDs prepared by the Langmuir-Blodgett technique. *Advanced Materials,* Vol.8, No.2, (February, 1996), pp. 146–149, ISSN 1521-4095

Friend, R.H.; Denton, G.J.; Halls, J.J.M.; Harrison, N.T.; Holmes, A.B.; Köhler, A.; Lux, A.; Moratti, S.C.; Pichler, K.; Tessler, N.; Towns, K. & Wittmann, H.F. (1997). Electronic excitations in luminescent conjugated polymers. *Solid State Communications*, Vol.102, No.2-3, (April, 1997), pp. 249-258, ISSN 0038-1098

Gobato, Y. G.; Marletta, A.; Faria, R. M.; Guimarães, F. E. G.; de Souza, J. M. & Pereira, E. C. (2002). Photoinduced photoluminescence intensity enhancement in poly(p-phenylene vinylene) films. *Applied Physics Letters*, Vol.81, No.5, (June, 2002), pp. 942-944, ISSN 0003-6951

Gua, X.; Raghavana, D.; Nguyenb, T.; VanLandinghamb, M.R & Yebassaa, D. (2001). Characterization of polyester degradation using tapping mode atomic force microscopy: exposure to alkaline solution at room temperature. *Polymer Degradation and Stability*, Vol.74, No.1, (September, 2001), pp. 139-149, ISSN 0141-3910

Holzera, W.; Penzkofera, A.; Pichlmaiera, M.; Bradleyb, D.D.C W. & Blauc J. (1999). Photodegradation of some luminescent polymers. *Chemical Physics*, Vol.248, No. 2-3, (December, 1999), pp. 273-284, ISSN 0301-0104

Kumar, J.; Li, L.; Jiang, X. L.; Kim, D.-Y.; Lee, T. S. & Tripathy, S. (1998). Gradient force: The mechanism for surface relief grating formation in azobenzene functionalized polymers. *Applied Physics Letters*, Vol.72, No.17, (February, 1998), pp. 2096-2098, ISSN 0003-6951

Magonov, S. N. & Whangbo M.-H. (1996). *Surface Analysis with STM and AFM: Experimental and Theoretical Aspects of Image Analysis,* Wiley-VCH, ISBN 978-3527293131, Weinheim, Federal Republic of Germany

Marletta, A.; Gonçalves, D.; Oliveira, O. N.; Faria, R. M. & Guimarães, F. E. G. (2000). Rapid Conversion of Poly(p-phenylenevinylene) Films at Low Temperatures. *Advanced Materials,* Vol.12, No.1, (January, 2000), pp. 69–74, ISSN 1521-4095

Marletta, A.; Vega, M. L.; Rodrigues, C. A.; Gobato, Y. G.; Costa, L. F. & Faria, R. M. (2009). Photo-irradiation effects on the surface morphology of poly(p-phenylene vinylene) films. *Applied Surface Science*, Vol.256, No.10, (March, 2010), pp. 3018–3023, ISSN 0169-4332

Marti, O.; Stifter, T.; Waschipky, H.; Quintus, M. & Hild, S. (1999). Scanning probe microscopy of heterogeneous polymers. *Colloids and Surfaces A: Physicochemical and Engineering Aspects*, Vol.154, No.1-2, (August, 1999), pp. 65-73, ISSN 0927-7757

Onoda, M; Manda, Y.; Iwasa, T.; Nakayama, H; Amakawa, K & Yoshino, K. (1990). Electrical, optical, and magnetic properties of poly(2,5-diethoxy-p-phenylene vinylene). *Physical Review B: condensed matter and materials physics*, Vol.42, No.18, (December, 1990), pp. 11826–11832, ISSN 1098-0121

Palasantzas, G. (1993). Roughness spectrum and surface width of self-afFine fractal surfaces via the K-correlation model. *Physical Review B: condensed matter an materials physics*, Vol.48, No.19, (May, 1993), pp. 14472-14478, ISSN 1098-0121

Simpson, G. J.; Sedin, D. L. & Rowlen, K. L. (1999). Surface Roughness by Contact versus Tapping Mode Atomic Force Microscopy. *Langmuir*, Vol.15, No.4, (January, 1999), pp. 1429–1434, ISSN 0743-7463

Therézio, E. M.; Piovesan, E.; Anni, M.; Silva, R. A.; Oliveira, O. N. & Marletta, A. (2011) Substrate/semiconductor interface effects on the emission efficiency of luminescent polymers. *Journal of Applied Physics*, Vol.110, No.4, (August, 2011), pp. 044504-044509, ISSN 1089-7550

Therézio, E. M.; Piovesan, E.; Vega, M. L.; Silva, R. A.; Oliveira, O. N. & Marletta, A. (2010). Thickness and annealing temperature effects on the optical properties and surface morphology of layer-by-layer poly(p-phenyline vinylene)+ dodecylbenzenesulfonate films. *Journal of Polymer Science Part B: Polymer Physics*, Vol.49, No.3, (February, 2011), pp. 206-213, ISSN 1099-0488

Thomas, T. R. (1999). *Rough Surfaces,* Imperial College Press, ISBN 978-1860941009, London, England

Weisenhorn, A. L.; Maivald, P.; Butt, H. J. & Hansma P. K. (1992). Measuring adhesion, attraction, and repulsion between surfaces in liquids with an atomic-force microscope. *Physical Review B: condensed matter and materials physics*, Vol.45, No.19, (May, 1992), pp. 11226–11232, ISSN 1098-0121

Zhao, Y.; Wang, G.-Ch. & Lu, T. M. (2001). *Characterization of amorphous and crystalline rough surface: principles and applications,* Academic Press, ISBN 0-12-475984-X, San Diego CA, USA

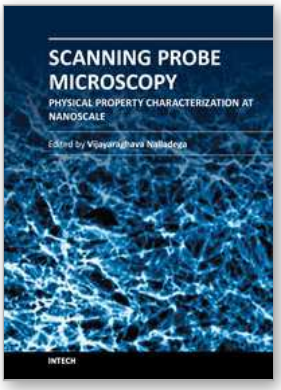

Scanning Probe Microscopy-Physical Property Characterization at Nanoscale

Edited by Dr. Vijay Nalladega

ISBN 978-953-51-0576-3
Hard cover, 242 pages
Publisher InTech
Published online 27, April, 2012
Published in print edition April, 2012

Scanning probe microscopy (SPM) is one of the key enabling tools for the advancement for nanotechnology with applications in many interdisciplinary research areas. This book presents selected original research works on the application of scanning probe microscopy techniques for the characterization of physical properties of different materials at the nanoscale. The topics in the book range from surface morphology analysis of thin film structures, oxide thin layers and superconducting structures, novel scanning probe microscopy techniques for characterization of mechanical and electrical properties, evaluation of mechanical and tribological properties of hybrid coatings and thin films. The variety of topics chosen for the book underlines the strong interdisciplinary nature of the research work in the field of scanning probe microscopy.

INTECH
open science | open minds

InTech Europe
University Campus STeP Ri
Slavka Krautzeka 83/A
51000 Rijeka, Croatia
Phone: +385 (51) 770 447
Fax: +385 (51) 686 166
www.intechopen.com

InTech China
Unit 405, Office Block, Hotel Equatorial Shanghai
No.65, Yan An Road (West), Shanghai, 200040, China
中国上海市延安西路65号上海国际贵都大饭店办公楼405单元
Phone: +86-21-62489820
Fax: +86-21-62489821